Temperature Dependence of Molecular Conformation in Solid-State Phase Transformations of N-Base Adducts of Bis(1,5-cyclooctanediyl)diboroxane by X-ray Diffraction

Mohamed Yalpani[a]*, Roland Köster[a], Roland Boese[b], and Martin Sulkowski[b]

Max-Planck-Institut für Kohlenforschung[a],
Kaiser-Wilhelm-Platz 1, D-4330 Mülheim an der Ruhr
Institut für Anorganische Chemie der Universität Essen[b],
Universitätsstraße 5–7, D-4300 Essen

Received June 6, 1988

Keywords: Crystal dynamics / Fluctional solids / N-Base–organoboron adducts / Phase transformations

The structures of the two adducts **P-1** and **Q-1** of bis(1,5-cyclooctanediyl)diboroxane (**1**) with pyridine (**P**) and quinuclidine (**Q**), which show solid-"solid" phase transformations at about 127 and 88°C, respectively, have been determined by X-ray diffraction at −145 and −163°C, respectively. The structure of **Q-1** has also been determined at room temperature and at +50°C. Both **P-1** and **Q-1** are packed in head-to-tail pairs and show extensive isothermal as well as temperature-dependent dynamics in the crystalline phase. The onset of transformations into the new "fluctional solid" phase is discussed in terms of these lattice packings and the observed translational and vibrational dynamics.

Röntgenstrukturanalyse und molekulare Dynamik von Festkörper-Phasenumwandlungen der N-Base-Addukte des Bis(1,5-cyclooctandiyl)diboroxans

Von zwei Lewis-Base-Addukten des Bis(1,5-cyclooctandiyl)diboroxans (**1**) (mit Pyridin: **P-1**; Quinuclidin: **Q-1**) mit Fest-„Fest"-Phasenumwandlungen bei 127 bzw. 88°C wurden Röntgenstrahlbeugungs-Strukturen bei −145 bzw. −163°C ermittelt. Von **Q-1** wurde zusätzlich die Struktur bei Raumtemperatur und bei +50°C bestimmt. **P-1** und **Q-1** sind im Gitter als Paare geordnet und zeigen umfangreiche isotherme und temperaturabhängige Dynamik in kristalliner Phase. Der Übergang in die neue, „fluktuierende Festkörper"-Phase wird unter Einbeziehung der Gitteranordnung, der beobachteten Intragitter-Translative und der vibrativen Bewegungsvorgänge diskutiert.

In the preceding paper[1] we showed that a number of N-bases readily form 1:1 adducts with tetraorganodiboroxanes R_2BOBR_2. In solutions, the base in these adducts appears to fluctuate between the two boron atoms of the diboroxane. The rate of these fluctuations is slowed down at lower temperatures, and the base seemingly comes to rest on one of the boron atoms. Exeption to these were the strongly basic tertiary amines triethylamine, tetramethylethylenediamine, and quinuclidine (**Q**) (pK_a = 10.8, 9.0, and 10.95[2]), which showed slight or no interaction when admixed at room temperature with bis(1,5-cyclooctanediyl)diboroxane (**1**). Yet complexation was observable in solutions of **Q** and **1** at very low temperatures (< −60 to −115°C), and from appropriate solvents a crystalline 1:1 adduct could be obtained. The stability of this adduct, evident by the relatively high melting point of 129°C, appeared to contrast to its ready dissociation into components in solution. Furthermore, the observation of an unusual premelting endothermic phase transformation of **Q-1** (DSC) and of the corresponding pyridine adduct **P-1** prompted us to investigate the solid state structures of these adducts by X-ray diffraction[3].

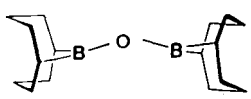

1

P

Q

Results and Discussion

Figures 1 and 2 show the results of the X-ray analysis of crystalline **P-1** (space group $P2_1/c$) and **Q-1** (space group $P2_1/n$) obtained at −145 and −163°C (LT), respectively. In the lattice of **P-1** there are two independent molecules. In Table 1, where some selected bond lengths and angles of **P-1** and **Q-1** are listed, the averaged values for the two molecules of **P-1** are shown. In both solids the base nitrogen atom is bonded to one of the boron atoms resulting in tetracoordination around the latter. This results in significant structural changes in the borabicyclic ring carrying the base (ring A) as compared to ring B with a trigonal boron atom. Thus besides the expected changes in the bond angles (cf. Table 1) at the sp^3-hybridized boron atom of ring A, the B–C bond lengths are elongated [ca. 1.61 Å (av.)] versus those of ring B [ca. 1.57 Å (av.)]. Also the B1–N1 bond length in **Q-1** of 1.717 Å (LT) is significantly elongated compared to the more common[1,4] B–N bond length of 1.66 Å (av.) in **P-1**. Both of the bicyclic rings in **P-1** and **Q-1** are deformed at the bridgehead carbon atoms C1 and C5 in ring A and C9 and C13 in ring B. Thus, the carbon atoms C6 and C8 of ring A which are adjacent to the coordinating base are apparantly pushed away from the base, causing a widening of the B1–C1–C8 and B1–C5–C6 angles to 112° (av.) for **P-1** and 114° (av.) for **Q-1** and thereby compressing the adjoined angles B1–C1–C2 and B1–C5–C4 to 106° (av.) for both **P-1** and **Q-1**. This tilting of the bicyclic

  0009–2940/89/0101–0009 $ 02.50/0

system of ring A away from the base apparantly causes a similar but with respect to the base opposite deformation in ring B. Thus, the angles B2–C9–C10 and B2–C13–C12 facing the base are now compressed to 106° (av.) while those on the far side (B2–C9–C16 and B2–C13–C14) are widened to 109° (av.) for **P-1** and 113° (av.) for **Q-1**.

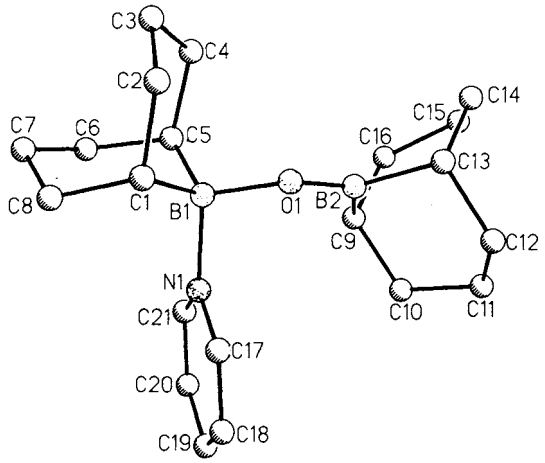

Figure 1. Molecular structure and atom numbering scheme of **P-1** (LT)

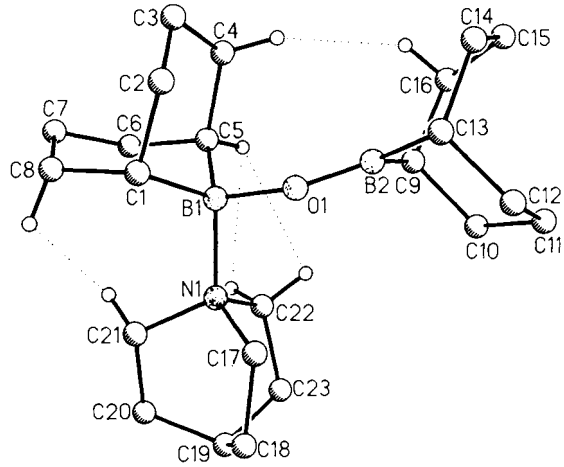

Figure 2. Molecular structure and atom numbering scheme of **Q-1** (LT). Dotted lines show short nonbonding intramolecular H···H distances

Rings A and B show also some angular distortions about their BO bonds, e.g., in ring B of **P-1** the O1–B2–C13 angle is significantly larger (128.1°) than the O1–B2–C9 angle (121.1°). For the same ring of **Q-1** the differences are slightly larger, 129.0° and 120.0°, respectively. Other angle distortions in ring A are also evident, especially in **Q-1** (cf. Table 1). Rings A and B in **P-1** and **Q-1** are also twisted with respect to each other. In **P-1** the torsional angle between B2–O1 and B1–N1 amounts to 64.4°. In **Q-1** this angle is increased to 100.6°.

Furthermore, the shortened B2–O1 bond [ca. 1.35 Å (av.)] in both **P-1** and **Q-1** points to extensive p orbital overlap of the nonbonded oxygen electron pair onto B2 and to the resulting π character of this bond. As a consequence the atoms B1, O1, B2, C9, and C13 should all lie in one plane. In fact the torsional angle between the atoms B1–O1 and B2–C13 for **P-1** is −9.6° and for **Q-1** 23.4°. It could therefore be expected that the B1–O1–B2 bond angle is of the order of 120°. The actual bond angles found are larger, 131.6° in **P-1** and 142.4° in **Q-1**.

Table 1. Selected bond lengths (Å) and angles (°) for **P-1** and **Q-1** (LT, RT, and HT = Low, Room, and High Temperature)

Bond/Angle	Q-1 (LT)	Q-1 (RT)	Q-1 (HT)	P-1*
B1–N1	1.717(2)	1.713(4)	1.665(18)	1.661(4)
B1–O1	1.481(2)	1.473(4)	1.505(15)	1.487(4)
B2–O1	1.349(2)	1.334(4)	1.360(15)	1.347(4)
B1–C1	1.654(2)	1.622(4)	1.667(18)	1.610(5)
B1–C5	1.641(2)	1.600(4)	1.649(16)	1.614(5)
B2–C9	1.610(2)	1.563(5)	1.559(18)	1.575(5)
B2–C13	1.588(3)	1.560(5)	1.539(23)	1.581(5)
B1–O1–B2	140.8(1)	142.4(2)	142.5(9)	132.5(3)
C1–B1–C5	105.1(1)	105.0(2)	101.5(9)	106.6(2)
C9–B2–C13	109.8(1)	109.8(3)	109.8(11)	110.7(3)
B1–C5–C6	113.2(1)	114.4(3)	112.4(11)	112.7(3)
B1–C1–C8	115.7(1)	115.2(3)	115.8(11)	110.5(3)
B1–C1–C2	105.2(1)	106.0(3)	107.8(10)	106.9(3)
B1–C5–C4	107.2(1)	106.5(3)	110.8(12)	106.0(3)
C2–C1–C8	110.0(1)	110.1(3)	109.3(12)	114.4(3)
C4–C5–C6	110.8(1)	110.7(3)	112.7(12)	112.4(3)
B2–C9–C10	105.2(1)	106.2(3)	105.0(10)	106.6(3)
B2–C13–C12	107.2(1)	106.5(3)	108.8(17)	105.9(3)
B2–C9–C16	110.4(1)	112.0(3)	113.2(13)	108.7(3)
B2–C13–C14	108.9(1)	105.1(3)	105.8(12)	108.9(3)
C10–C9–C16	113.4(1)	112.3(3)	112.9(12)	114.6(3)
C12–C13–C14	114.4(1)	114.4(3)	111.8(14)	114.3(3)
O1–B1–C1	108.4(1)	107.9(2)	104.9(10)	110.2(2)
O1–B1–C5	113.0(1)	115.0(2)	112.0(10)	108.2(2)
O1–B1–N1	102.8(1)	101.3(2)	103.3(8)	103.3(2)
C1–B1–N1	112.8(1)	113.1(2)	115.1(9)	110.1(2)
C5–B1–N1	114.8(1)	114.6(2)	119.4(11)	112.5(2)
O1–B2–C9	129.0(1)	130.1(3)	131.7(12)	128.1(3)
O1–B2–C13	120.9(1)	119.9(3)	118.5(11)	121.1(3)

* Averaged values of the two molecules of **P-1** in the unit cell (weighted r.m.s. deviations = 0.1589 Å for the two structures).

For comparison, the B–O–B angles found in various free diboroxanes are: For $(Me_2B)_2O$ (in the solid state dimeric[5]) in the gas phase it is 144.4° (electron diffraction)[6]; for sterically more crowded molecules which are more similar to **1**, such as tetramesityldiboroxane[7], $(C_{14}H_{12}B_2)_2O$[8], and $(C_{10}H_6B_2S_2)_2O$[9], the angles found are 165.5, 159.4, and 152.6°, respectively. The larger angle found in **Q-1** is thus close to that expected for free **1**.

The closeness of the base nitrogen atom to both boron atoms of the diboroxane molecule, a necessity for a fluctuating system in solution, continues in the solid state. This can be clearly seen from the conformation that ring B adopts around the O1–B1 single bond. Of all the possible rotational conformations, some of which should sterically be even more favourable, it has adopted the one in which B2 is nearest to the nitrogen atom of the base. The close approach of the nitrogen atom to both of the boron atoms in

the solid state, as we shall see below, subjects the molecule to severe sterical strains and suggests that the fluctuation continues up to the final moments before crystallization sets in.

This can perhaps be seen in the premelting behaviour of crystals of **P-1** (m.p. 129–131°C) and of **Q-1** (m.p. 123–125°C). In both cases the crystals, viewed under a microscope during the melting point determination, began an internal sintering accompanied by loss of refractivity at about 120 and 90°C, respectively. An opaque and waxy texture developed without actually melting and thereby changing the external morphology of the crystals. Below the melting point, when kept at a constant temperature, this appearance does not change noticeably. To investigate this phenomenon more closely, differential thermal scans (DSC) were performed. These are shown in Figures 3a and 4a. It can be seen that a large endothermic event (31.1 kJ/mol) starting at about 120°C for **P-1** and at about 90°C (51.3 kJ/mol) for **Q-1** preceeds the final melting processes. The large ratios of the premelting endothermic transitions to the relatively small melting enthalpies (ca. 10:1 for **P-1** and ca. 3:1 for **Q-1**) as well as the visual appearance of these "solids" in the intervening temperature range are reminiscent of properties of liquid or plastic crystals. We interpret this process as an onset of intramolecular motion (fluctuation of the amine molecule between the boron atoms of the diboroxane) without a significant movement of the molecules away from their intralattice positions. The transition temperatures starting at about 129–131°C for **P-1** and 123–125°C for **Q-1** are, therefore, not melting points in the usual sense, rather they may be considered to be the clearing points associated with liquid crystallinity.

It is also interesting to consider the cooling to and the subsequent reheating processes of these "solids" formed from their respective melts (cf. Figures 3b and 4b). For **P-1** which on cooling does not crystallize, an exothermic reorganizational event (crystallization?) is observed on reheating at about 50°C (cf. Figure 3b). The amount of heat released during this event is only a third of that absorbed for the premelting and melting transformations. On further heating the premelting and melting (clearing) transitions appear combined at about 135°C, absorbing the same amount of heat as during the virgin heating scan for both the premelting and melting processes. This shows that the prior reorganization is on the whole a gradual and uneventful process. For **Q-1** cooling brings about a reversal of the events observed during the heating scan (cf. Figure 4b). Initially, a low-energy "crystallization" showing supercooling is followed by a more energetic reorganizational transformation with a hysteresis of about 42°C[10]. A reheating scan shows the complete reversibility in this case (cf. Figure 4a).

Surprisingly, it was found that these transformations are unique to **P-1** and **Q-1**. Other 1:1 adducts of N-bases with **1**, such as those described in the preceding paper[1], and the 1:2 adducts of 4,4′-bipyridyl and 4,4′-trimethylenedipyridine with **1**, showed only a melting transition[11]. These melting points generally showed an increase roughly parallel to the rise of the pK_a's of the N-bases (e.g. for **P-1** 133°C, 4-

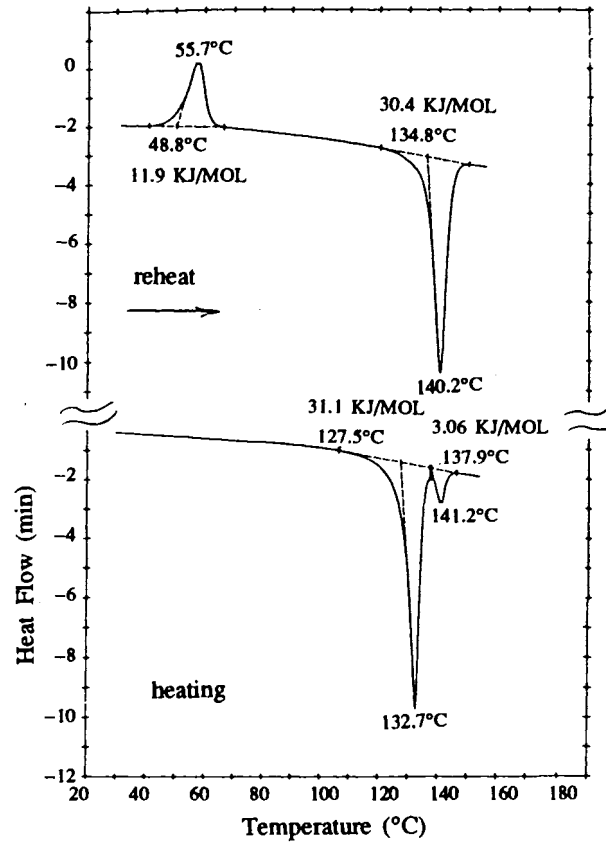

Figure 3. DSC scans of **P-1**: (a) virgin, (b) reheat

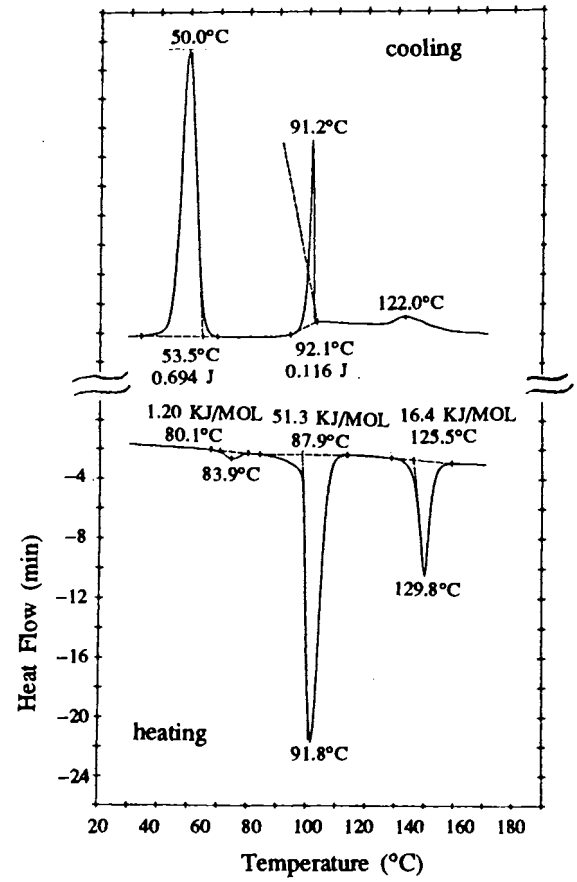

Figure 4. DSC scans of **Q-1** (a) heating, (B) cooling

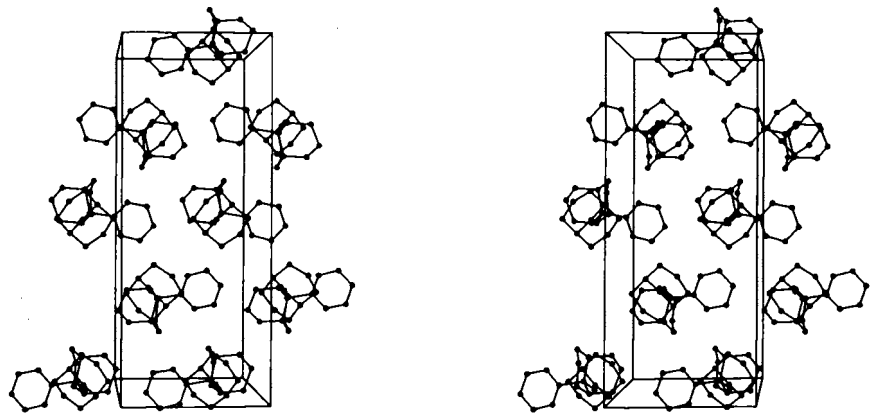

Figure 5. Stereoscopic view of molecular packing of **P-1**

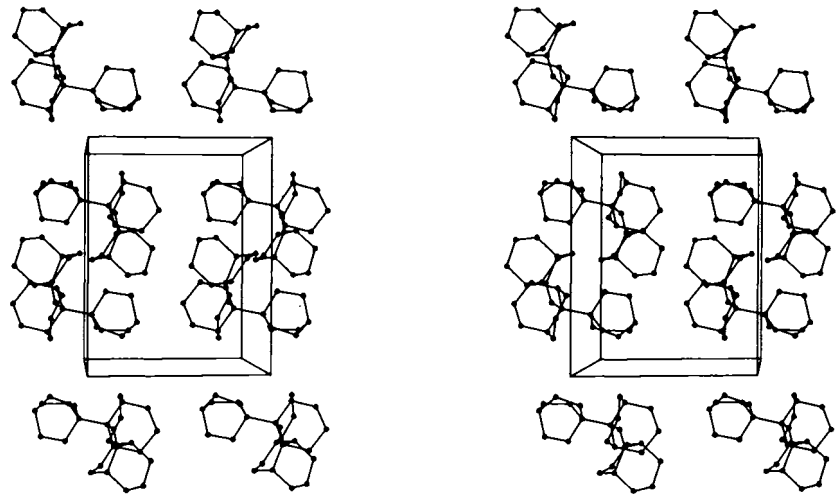

Figure 6. Stereoscopic view of molecular packing of **Q-1**

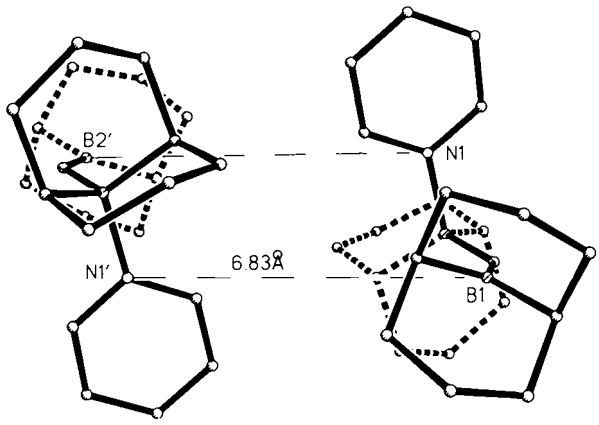

Figure 7. Pairing of molecules in the lattice of **P-1**

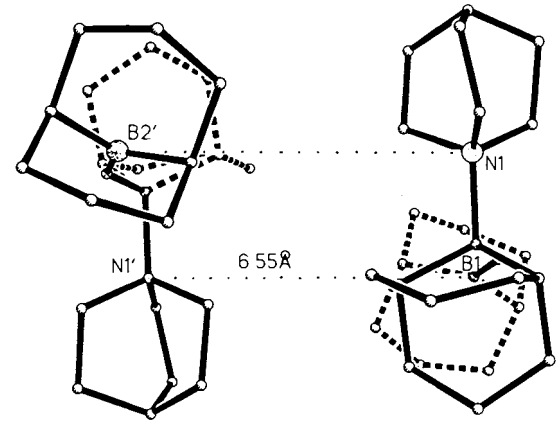

Figure 8. Pairing of molecules in the lattice of **Q-1**

methyl-**P-1** 147 °C, 3,5-dimethyl-**P-1** 164 °C, and 4-dimethylamino-**P-1** 232 °C). Obviously, the B – N bond strength in these complexes appear to have a direct influence on their respective lattice stabilities and would suggest that it is the rupture of this bond which results in the melting (clearing) transitions.

Q-1 has the lowest melting point in this series and as mentioned above is completely dissociated in solutions at moderate temperatures[1]. We attribute this to the severe strains experienced by a tertiary amine as it becomes engulfed by the bulky environment of **1**. The effect of these strains are clearly evident from the comparison of some of

the bond lengths and angles in molecules of **Q-1** and **P-1** (cf. above). Additional indications for the increase in internal crowding in **Q-1** compared to **P-1** are some of the extremely short intramolecular H···H distances, some of which are

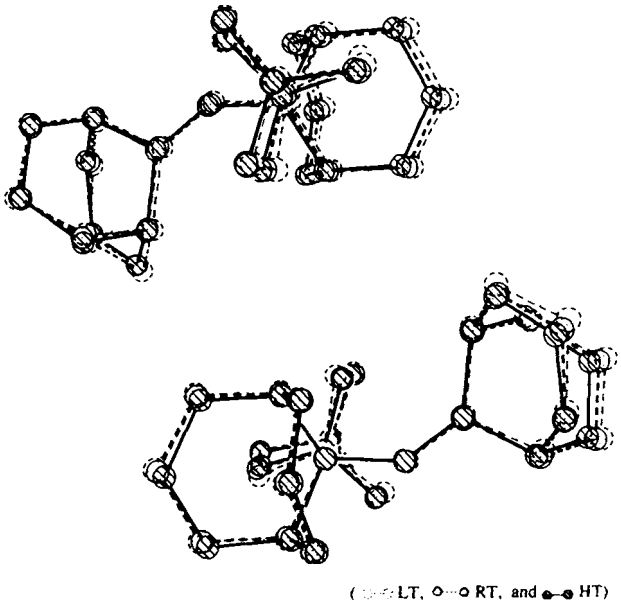

Figure 9a. Superimposition of pairs of the three LT, RT, and HT structures of **Q-1**. View on the B1 – N1 axis and along the B1 – O1 bond

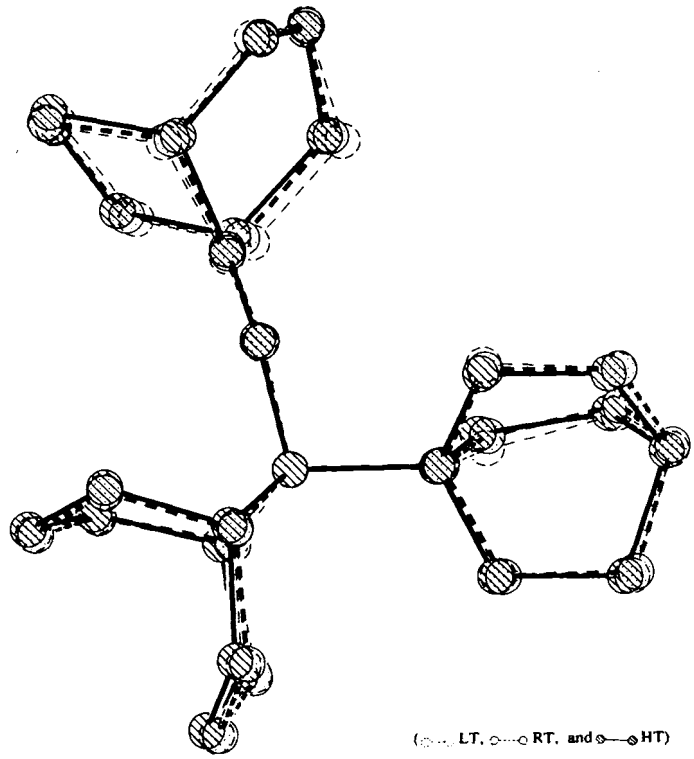

Figure 9b. Superimposition of the three LT, RT, and HT structures of **Q-1**. View on the N1, B1, and O1 plane

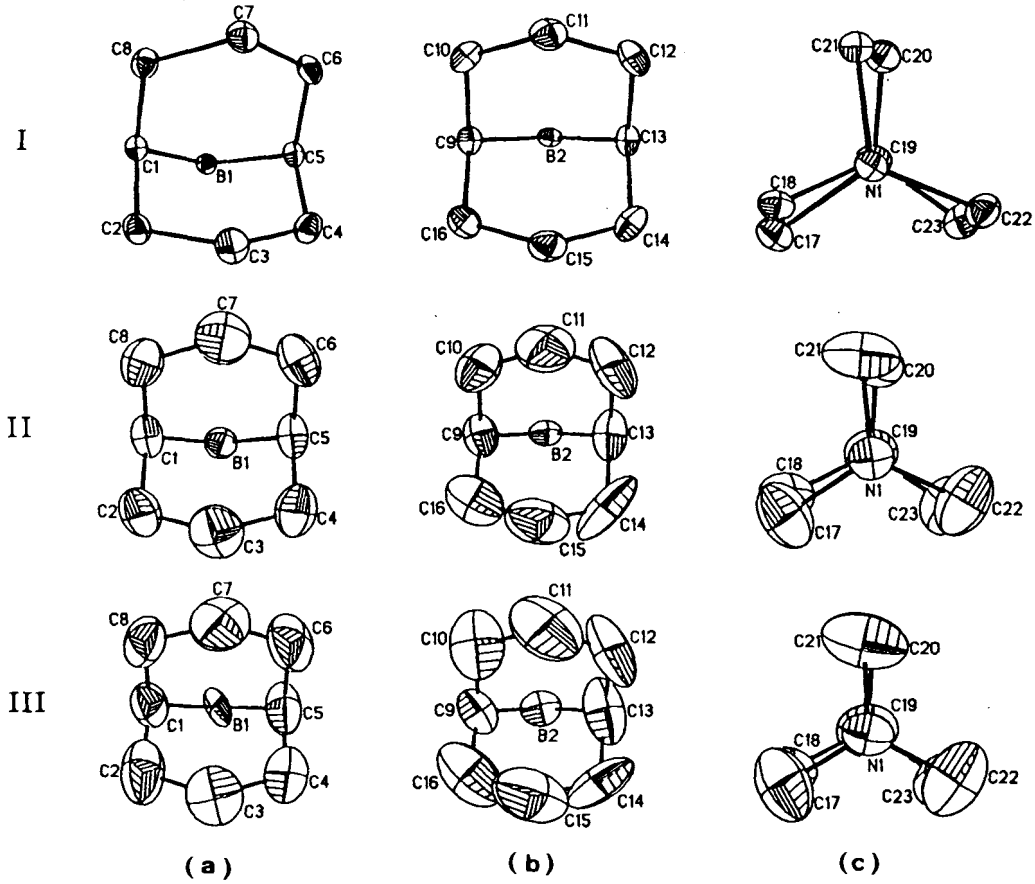

Figure 10. ORTEP drawings displaying vibrational ellipsoids (50% probability levels) of (a) **Q-1** (HT); (b) end-on views of ring A, ring B, and (c) top-on view of the **Q** segments of **Q-1** (RT)

closely bordering at, e. g. H5 – H22 and H4 – H14, and some are within, e. g. H6 – H21, the van-der-Waal's radii calculated for two hydrogen atoms (cf. Figure 2).

The combination of these high intramolecular strains in **Q-1**, compared to **P-1** weakens the lattice structure and probably also contributes to the lowering of the transition temperatures to the new "solid" phase in the former. An insight into the processes causing the transitions into these new phases may be gained through the intralattice packings of molecules of **P-1** and **Q-1** shown in the stereo plots of Figures 5 and 6.

It can be seen that in both systems the molecules are arranged in head-to-tail pairs. Figures 7 and 8 each depict one pair of **P-1** and one of **Q-1**, respectively. In these one base molecule is bonded from above and another from below the plane of the pair. It can easily be envisaged that in the new solid phase the molecules gain some mobility about their lattice points, and these pairs (N1 – B2′ intermolecular distance ca. 6.5 Å for **Q-1** and 6.8 Å for **P-1**) move closer to each other and thereby enable the fluctuation of the base to also occur intermolecularly between the boron atoms of the neighbouring molecules. We suspect that it is this fast intermolecular to-and-fro motion of the base between neighbouring molecular pairs which connects the molecules and thereby maintains a semblance of order within the new "solid" phase.

Although the resulting phase has similarities in appearance to liquid, plastic[12], or conformationally disordered (condis)[13] crystalline phases, it has a different molecular basis and should, if the mechanism proposed above holds, be appropriately referred to as a fluctional crystalline phase.

Indications for the correctness of the above hypothesis should be obtainable from the analysis of temperature-dependent molecular motions in the solid state. We therefore determined additionally the solid-state structures of **Q-1** at room temperature (RT) and at +50 °C (HT), i.e., close to the transition temperature.

The result shows numerous and significant changes in the bond lengths and angles as the temperature is raised up to +50 °C. The pertinent data are also shown in Table 1. The most surprising of these changes, and contrary to a priori expectations, is the considerably shortened B1 – N1 bond

Table 2. Crystallographic data for **Q-1** (LT), **Q-1** (RT), **Q-1** (HT), and **P-1** (LT) and data collection procedures

	Q-1 (LT)	**Q-1** (RT)	**Q-1** (HT)	**P-1** (LT)
Formula	$C_{23}H_{41}B_2NO$	$C_{23}H_{41}B_2NO$	$C_{23}H_{41}B_2NO$	$C_{21}H_{33}B_2NO$
Crystal size (mm)	0.52x0.43x0.29	0.34x0.28x0.15	0.48x0.41x0.32	0.33x0.28x0.21
Space group	$P2_1/n$	$P2_1/n$	$P2_1/n$	$P2_1/c$
Z	4	4	4	8
a (Å)	9.862(2)	9.989(2)	9.986(2)	9.011(2)
b (Å)	12.516(2)	12.681(3)	12.735(3)	22.145(7)
c (Å)	17.053(4)	17.200(4)	17.2.04(3)	19.634(6)
β (deg)	97.01(2)	96.96(2)	96.85(2)	94.48(2)
T (K)	110	298	323	128
V (Å^3)	2088.9(7)	2165.3(7)	2172.3(7)	3906.0(2)
d_{calcd} (g/cm^3)	1.17	1.13	1.13	1.15
μ (cm^{-1})	0.70	0.70	0.70	0.63
Radiation	Mo–K_α	Mo–K_α	Mo–K_α	Mo–K_α
$2\Theta_{max}$ (deg)	50	50	40	45
Total no. of unique reflections	3686	3769	1992	5107
Observed reflections [$F_o \geq 4\sigma(F)$]	3359	2385	1191	3654
R	0.049	0.072	0.119	0.060
$R_w[w^{-1} = \sigma^2(F_o) + g(F_o^2)]$	0.068	0.082	0.133	0.061
g	61.6 x 10^{-4}	29.0 x 10^{-4}	2.2 x 10^{-4}	7.6 x 10^{-4}
Residual electron density (e/Å^3)	0.74	0.38	0.36	0.35

(1.665 Å at HT compared to 1.717 Å at LT). An inspection of alterations of bond angles around the tetracoordinated boron atom shows that the angles O1 – B1 – C1 and O1 – B1 – C5 have become smaller while the adjoining angles O1 – B1 – N1, C1 – B1 – N1, and C5 – B1 – N1 have all widened. These, together with the lengthening of the B1 – O1, B1 – C1, and B1 – C5 bonds and other alterations in bond lengths and angles, make the environment on the side of the quinuclidine moiety become less crowded and therefore allows a closer approach of **Q** to B1. This bond is now of a similar magnitude as the corresponding one in **P-1**. It is obvious that these bond and angle changes around B1 will result in positional movements of the atoms in other parts of the molecule. These alterations are shown in Figures 9 and 10.

Figure 9a presents a projection from above and is a superimposition of the three LT, RT, and HT structures. To demonstrate the intra- and intermolecular static translational changes at each of the three temperatures we have anchored one of the pairs of **Q-1** on the axis of the B1 – N1 and along the length of the B1 – O1 bond. The Figure clearly shows the positional changes of the atoms within one molecule and also the very significant shift of the second molecule of the pair as the temperature is raised from −163 to +50 °C. This Figure also demonstrates that all movements occur only along the B – O – B molecular axis and that there are essentially no movements along the orthogonal direction, which demonstrates that these changes are irrespective of the normal temperature-dependent expansion of the lattice. Figure 9b is a side-on projection on the plane made up of the three atoms N1, B1, and O1 and the superimposition of the LT, RT, and HT structures. It likewise shows the relative variation in molecular geometry at the three temperatures.

A different approach for investigating molecular dynamics in the solid state and phase transformations is the analysis of anisotropic atomic displacement parameters[14]. Figure 10 depicts the 50% thermal ellipsoids of **Q-1** at LT (I), RT (II), and HT (III). It clearly shows the cooperative libratory motions of the two borabicyclic rings as well as that of the quinuclidine moiety which significantly increase as the temperature rises.

In Figure 10 the partial structures (a – c) depict the top-on projections on the plane comprising the atoms C2, C4, C6, C8 of the tetracoordinated borabicyclic ring, a similar view on the corresponding tricoordinated ring, and the top-on projection on the quinuclidine moiety, respectively. Additionally, Figure 10c shows beside the libration of the fron-

Table 3. Atomic coordinates (× 10^4) and equivalent isotropic displacement factors (Å^2 × 10^3) for **Q-1** (LT)

	x	y	z	U_{eq}
O(1)	8230(1)	2978(1)	6234(1)	16(1)*
N(1)	10344(1)	2416(1)	5691(1)	15(1)*
B(1)	8650(2)	2675(1)	5465(1)	13(1)*
B(2)	7984(2)	3843(1)	6654(1)	16(1)*
C(1)	7773(2)	1620(1)	5140(1)	16(1)*
C(2)	6270(2)	1908(1)	5205(1)	21(1)*
C(3)	5759(2)	2888(1)	4707(1)	25(1)*
C(4)	6751(2)	3846(1)	4768(1)	22(1)*
C(5)	8292(2)	3580(1)	4788(1)	16(1)*
C(6)	8622(2)	3230(1)	3966(1)	20(1)*
C(7)	7937(2)	1274(1)	4286(1)	19(1)*
C(8)	7949(2)	2173(1)	3665(1)	23(1)*
C(9)	8598(2)	5017(1)	6613(1)	19(1)*
C(10)	9585(2)	5146(1)	7387(1)	23(1)*
C(11)	8958(2)	4934(1)	8152(1)	26(1)*
C(12)	8062(2)	3926(2)	8133(1)	29(1)*
C(13)	7092(2)	3768(1)	7360(1)	21(1)*
C(14)	5927(2)	4595(2)	7229(1)	29(1)*
C(15)	6379(2)	5750(2)	7101(1)	27(1)*
C(16)	7439(2)	5853(1)	6523(1)	25(1)*
C(17)	10601(2)	1897(1)	6493(1)	18(1)*
C(18)	12078(2)	1496(1)	6672(1)	20(1)*
C(19)	12950(2)	2073(1)	6124(1)	21(1)*
C(20)	12518(2)	1670(1)	5286(1)	21(1)*
C(21)	10947(2)	1674(1)	5129(1)	17(1)*
C(22)	11157(2)	3438(1)	5726(1)	18(1)*
C(23)	12612(2)	3268(1)	6140(1)	23(1)*

* Equivalent isotropic U defined as one third of the trace of the orthogonalized U_{ij} tensor.

Table 4. Atomic coordinates (× 10^4) and equivalent isotropic displacement factors (Å^2 × 10^3) for **Q-1** (RT)

	x	y	z	U_{eq}
O(1)	8266(2)	3004(2)	6249(1)	44(1)*
N(1)	10344(2)	2450(2)	5707(1)	36(1)*
B(1)	8656(3)	2711(3)	5476(2)	38(1)*
B(2)	8016(3)	3837(3)	6686(2)	40(1)*
C(1)	7786(3)	1677(2)	5168(2)	47(1)*
C(2)	6308(3)	1959(3)	5219(2)	60(1)*
C(3)	5829(4)	2934(3)	4734(3)	70(1)*
C(4)	6802(4)	3862(3)	4797(2)	61(1)*
C(5)	8320(3)	3581(2)	4804(2)	47(1)*
C(6)	8613(4)	3230(3)	3993(2)	64(1)*
C(7)	7974(5)	2184(3)	3711(2)	71(2)*
C(8)	7969(4)	1314(3)	4329(2)	58(1)*
C(9)	8501(4)	5009(3)	6645(2)	59(1)*
C(10)	9482(4)	5200(4)	7398(3)	79(2)*
C(11)	8995(5)	4895(5)	8135(2)	102(2)*
C(12)	8194(6)	3906(4)	8141(2)	106(2)*
C(13)	7200(4)	3692(3)	7400(2)	71(2)*
C(14)	5960(4)	4534(5)	7256(4)	119(2)*
C(15)	6370(6)	5626(5)	7084(3)	107(2)*
C(16)	7345(5)	5769(3)	6567(3)	92(2)*
C(17)	10579(3)	1848(3)	6462(2)	63(1)*
C(18)	12033(4)	1504(3)	6665(2)	58(1)*
C(19)	12906(3)	2104(3)	6147(2)	59(1)*
C(20)	12512(3)	1740(3)	5314(2)	61(1)*
C(21)	10995(4)	1797(4)	5124(2)	70(1)*
C(22)	11127(4)	3450(3)	5820(3)	67(1)*
C(23)	12582(3)	3261(3)	6193(3)	68(1)*

* Equivalent isotropic U defined as one third of the trace of the orthogonalized U_{ij} tensor.

tal three atoms C17, C21, and C22 also a precession of the end section of **Q**, best evident by the large, nearly circular ellipsoid of C19 visible behind N1.

Both of these methods of variable-temperature and isothermal analyses, although indicative of extensive intra- and intermolecular dynamics in the solid state, provide no clues on the nature of molecular movements past the transition. Unfortunately, structure analysis nearer to the transition temperature was impossible due to gradual "deterioration" of the crystal quality during the long data aquisition time even at the +50°C measurement. Therefore, information about this new "fluctionally crystalline" state must await application of other techniques such as powder diffraction or solid-state NMR spectroscopy.

Experimental

Instruments: Büchi melting point apparatus and Leitz Dialux 20 Hotstage microscope, scaled capillary tubes. – DSC analyses: DuPont 1090.

The preparation of pyridine- and quinuclidine-bis(1,5-cyclooctanediyl)diboroxanes **P-1** and **Q-1** are described in the preceding paper[1].

X-Ray Single-Crystal Structure Determination of **P-1** *and* **Q-1** *(General Procedure):* Data collection and calculations were carried out on a Syntex R-3 m/V four-circle diffractometer with a Microvax II computer and SHELXTL-PLUS software[15]. The structure solutions were obtained by direct methods, and hydrogen atoms were included as rigid groups (C–H bond length at 0.96 Å, C–C–H and H–C–H angles of 109.5 and 120°, respectively). The isotropic atomic displacement parameters (IDP's) of the H atoms were re-

Table 5. Atomic coordinates (× 10^4) and equivalent isotropic displacement factors (Å^2 × 10^3) for **Q-1** (HT)

	x	y	z	U_{eq}
O(1)	8293(9)	3003(5)	6251(4)	70(3)*
N(1)	10397(11)	2458(6)	5712(4)	59(4)*
B(1)	8761(15)	2713(9)	5478(7)	52(5)*
B(2)	8062(16)	3840(10)	6706(8)	61(5)*
C(1)	7816(17)	1685(9)	5166(7)	77(6)*
C(2)	6394(22)	1954(10)	5225(8)	113(9)*
C(3)	5860(16)	2962(11)	4729(8)	97(6)*
C(4)	6867(16)	3871(10)	4800(9)	88(6)*
C(5)	8294(20)	3585(9)	4792(7)	87(7)*
C(6)	8598(19)	3234(10)	3994(7)	104(8)*
C(7)	7972(17)	2187(10)	3717(6)	97(7)*
C(8)	7958(16)	1309(8)	4322(7)	88(6)*
C(9)	8455(16)	5011(9)	6658(7)	77(6)*
C(10)	9451(20)	5215(11)	7404(8)	127(9)*
C(11)	8976(23)	4835(16)	8127(8)	152(11)*
C(12)	8190(25)	3877(13)	8127(8)	134(10)*
C(13)	7290(21)	3661(10)	7419(8)	113(9)*
C(14)	5999(15)	4477(14)	7310(12)	125(8)*
C(15)	6367(22)	5526(18)	7093(11)	158(12)*
C(16)	7278(22)	5722(11)	6589(10)	136(10)*
C(17)	10593(14)	1836(12)	6449(7)	84(6)*
C(18)	11988(16)	1526(11)	6652(7)	90(7)*
C(19)	12935(13)	2087(9)	6151(7)	75(5)*
C(20)	12506(18)	1741(11)	5313(7)	100(8)*
C(21)	11047(14)	1881(13)	5131(8)	91(6)*
C(22)	11117(15)	3455(10)	5853(9)	88(6)*
C(23)	12553(15)	3267(10)	6178(8)	91(6)*

* Equivalent isotropic U defined as one third of the trace of the orthogonalized U_{ij} tensor.

Table 6. Atomic coordinates (× 10^4) and equivalent isotropic displacement factors (Å^2 × 10^3) for **P-1** (LT)

	x	y	z	U_{eq}
O(1)	7399(2)	2086(1)	7369(1)	17(1)
B(1)	8071(4)	2425(2)	6816(2)	15(1)
B(2)	7504(4)	2161(2)	8053(2)	16(1)
N(1)	9878(3)	2305(1)	6976(1)	16(1)
C(1)	7524(3)	2151(1)	6079(2)	19(1)
C(2)	5811(3)	2200(1)	6001(2)	22(1)
C(3)	5162(4)	2825(2)	6140(2)	22(1)
C(4)	5928(3)	3158(2)	6757(2)	21(1)
C(5)	7644(3)	3133(1)	6794(2)	16(1)
C(6)	8279(4)	3474(1)	6199(2)	23(1)
C(7)	8067(4)	3163(2)	5498(2)	29(1)
C(8)	8303(4)	2476(2)	5518(2)	26(1)
C(9)	8589(3)	2591(1)	8495(2)	19(1)
C(10)	9677(4)	2175(2)	8921(2)	28(1)
C(11)	8967(4)	1677(2)	9318(2)	31(1)
C(12)	7659(4)	1357(2)	8945(2)	29(1)
C(13)	6550(3)	1765(1)	8522(2)	20(1)
C(14)	5624(4)	2191(2)	8948(2)	30(1)
C(15)	6507(4)	2688(2)	9340(2)	30(1)
C(16)	7651(4)	3007(2)	8930(2)	28(1)
C(17)	10373(3)	1732(1)	6951(2)	20(1)
C(18)	11830(3)	1575(2)	7119(2)	23(1)
C(19)	12839(4)	2024(2)	7324(2)	25(1)
C(20)	12347(3)	2610(1)	7354(2)	22(1)
C(21)	10871(3)	2733(1)	7177(2)	19(1)
O(2)	7684(2)	-114(1)	2696(1)	17(1)
B(3)	7016(4)	190(2)	3276(2)	16(1)
B(4)	7570(4)	-23(2)	2016(2)	18(1)
N(2)	5196(3)	65(1)	3115(1)	17(1)
C(51)	7610(3)	-128(1)	3984(2)	20(1)
C(52)	9323(3)	-66(1)	4038(2)	22(1)
C(53)	9918(4)	581(2)	3970(2)	25(1)
C(54)	9105(4)	953(2)	3399(2)	24(1)
C(55)	7392(3)	900(1)	3361(2)	19(1)
C(56)	6722(4)	1177(2)	3987(2)	26(1)
C(57)	6993(4)	823(2)	4663(2)	34(1)
C(58)	6846(4)	140(2)	4586(2)	28(1)
C(59)	8487(3)	-416(1)	1528(2)	20(1)
C(60)	7347(4)	-806(2)	1090(2)	26(1)
C(61)	6057(4)	-453(2)	725(2)	26(1)
C(62)	5356(4)	19(2)	1170(2)	23(1)
C(63)	6490(3)	426(1)	1587(2)	20(1)
C(64)	7420(4)	835(2)	1153(2)	26(1)
C(65)	8560(4)	518(2)	735(2)	28(1)
C(66)	9427(4)	10(2)	1109(2)	26(1)
C(67)	4707(3)	-508(1)	3121(2)	21(1)
C(68)	3257(3)	-666(2)	2938(2)	23(1)
C(69)	2241(4)	-216(1)	2741(2)	23(1)
C(70)	2738(3)	375(1)	2736(2)	23(1)
C(71)	4218(3)	496(1)	2923(2)	19(1)

fined without constraints. Structural data for **Q-1** (LT), (RT), and (HT) and **P-1** (LT) are shown in Table 2, and the atom coordinates in Tables 3–6[16].

CAS Registry Numbers

P-1: 116972-69-1 / **Q-1**: 116996-19-1

---

[1] M. Yalpani, J. Serwatowski, R. Köster, *Chem. Ber.* **121** (1988) 3, preceding paper.
[2] D. D. Perrin, *Dissociation Constants of Organic Bases in Aqueous Solutions*, Butterworth, London 1965.
[3] A crystal structure analysis of **P-1**, carried out by R. Köster, J. Serwatowski, and C. Krüger in 1982, had, limited by the crystal quality, resulted in a low-resolution structure solution ($R \approx 0.2$). From this partial solution it could be deduced that pyridine is bonded to one of the boron atoms of **1** [cf., R. Köster in *Methoden der Organischen Chemie* (Houben-Weyl-Müller), vol. XIII/3b (R. Köster, Ed.), p. 621, Thieme, Stuttgart 1983].
[4] M. Yalpani, R. Boese, R. Köster, *Chem. Ber.* **121** (1988) 287; C. Krüger, Y. H. Tsay, unpublished results (1982).
[5] H. Borrmann, A. Simon, H. Vahrenkamp, *Angew. Chem.*, in press.
[6] G. Gunderson, H. Vahrenkamp, *J. Mol. Struct.* **33** (1976) 97.
[7] C. J. Cardin, H. E. Parge, J. W. Wilson, *J. Chem. Res. (S)* **1983** 93.
[8] I. Cynkier, N. Furmanova, *Cryst. Struct. Commun.* **9** (1980) 307.
[9] B. Aurivillius, *Acta Chem. Scand., Ser. B*, **28** (1974) 998.
[10] M. Yalpani, W. R. Scheidt, K. Seevogel, *J. Am. Chem. Soc.* **107** (1985) 1684.
[11] We are currently investigating the solid-state structures of some of these adducts.
[12] B. Denise, P. Depond, M. Debean, P. Schweiss, *J. Physique* **48** (1987) 615.
[13] B. Wunderlich, M. Möller, H. G. Wiedemann, *Mol. Cryst. Liq. Cryst.* **140** (1986) 211.
[14] J. D. Dunitz, *Trans. Am. Cryst. Assoc.* **20** (1984) 1.
[15] G. M. Sheldrick, SHELXTL-PLUS (Version 1987), an *Integrated System for Solving, Refining, and Displaying Crystal Structures from Diffraction Data*, University of Göttingen.
[16] Further details of the crystal structure investigations are available on request from the Fachinformationszentrum Energie, Physik, Mathematik GmbH, D-7514 Eggenstein-Leopoldshafen 2, on quoting the depository number CSD-53352, the names of the authors, and the journal citation.

[149/88]